$(LaCoO_{3})_{n}/(SrCoO_{2.5})_{n}$ superlattices: Tunable ferromagnetic insulator

S. J. Noh, G. H. Ahn, J. H. Seo, Zheng Gai, Ho Nyung Lee, Woo Seok Choi, and S. J. Moon

Phys. Rev. B **100**, 064415 — Published 22 August 2019

DOI: 10.1103/PhysRevB.100.064415

$(LaCoO_3)_n/(SrCoO_{2.5})_n$ Superlattices: Tunable Ferromagnetic Insulator

S. J. Noh[1], G. H. Ahn[1], J. H. Seo[1], Zheng Gai[2], Ho Nyung Lee[3], Woo Seok Choi[3,4,*], and S. J. Moon[1,†]

[1]*Department of Physics, Hanyang University. Seoul 04763, Korea*

[2]*Center for Nanophase Materials Science, Oak Ridge National Laboratory, Oak Ridge, TN 37831, USA*

[3]*Materials Science and Technology Division, Oak Ridge National Laboratory, Oak Ridge, TN 37831, USA*

[4]*Department of Physics, Sungkyunkwan University, Suwon 16419, South Korea*

Ferromagnetic insulators have great potential for spintronic applications. For such applications, it is essential to find materials with a robust and controllable ferromagnetic insulating phase. However, because ferromagnetism in functional transition metal oxides is usually coupled to metallicity, ferromagnetic insulators are very rare and independent control of their magnetic and electrical properties is difficult. In this study, the electrical, magnetic, and optical properties of $(LaCoO_3)_n/(SrCoO_{2.5})_n$ superlattice films are investigated for the manipulation of the ferromagnetic insulating phase. Whilst the superlattices remain insulating irrespective of the periodicity n, the electronic structure and magnetic state vary drastically. Superlattices with large periodicities n of 10 and 20 show a ferromagnetic transition at a critical temperature T_C of ~80 K. With decreasing periodicity and increasing interface density of the superlattices, systems with n = 4 become almost nonmagnetic, while in systems with n = 2 and 1, a reentrant ferromagnetic phase is observed at T_C of ~180 and ~225 K, respectively. Optical spectroscopy reveals that the fine control of the magnetic ground state is achieved by the modified electronic structure associated with the spin-state transition. Our results suggest an important design principle to create and manipulate the ferromagnetic insulating properties of Co-based oxide thin films.

* choiws@skku.edu

† soonjmoon@hanyang.ac.kr

I. INTRODUCTION

Ferromagnetic insulators are essential components in viable spintronic applications, e.g., they can serve as spin-filtering tunneling barriers for tunneling magnetoresistance devices [1-4]. Transition metal oxides, including yttrium iron garnet ($Y_3Fe_2(FeO_4)_3$) and epitaxially strained $LaCoO_3$, exhibit both ferromagnetic and insulating behaviors, which are not commonly observed within a single material, making them some of the most promising ferromagnetic insulators [3,5-7]. The tunability of ferromagnetism in such materials, if possible, would further expand their practicality in spintronic devices.

$La_{1-x}Sr_xCoO_{3-\delta}$ (LSCO) is an interesting system with potential to achieve tunable ferromagnetic insulating properties. A delicate balance between the crystal field and the exchange interactions enables us to manipulate the spin states by means of various external perturbations, such as changes in temperature, charge-carrier doping, and/or epitaxial strains. On the one hand, perovskite $LaCoO_3$ (x = 0, LCO) epitaxial thin films grown on $SrTiO_3$ (STO) substrates are prominent ferromagnetic insulators with a critical temperature of ~85 K [6-9]. The tensile strain imposed in the thin films suppresses the bulk monoclinic distortions and stabilizes the robust ferromagnetic states [6,9,10]. Tensile-strained LCO film is a rare example of undoped ferromagnetic insulator with high-transition temperature (T_C) and high-symmetry structure. These characteristics enable epitaxial integration of the LCO film with common substrates or oxide films, which is highly beneficial for fabricating magnetic devices [11]. On the other hand, the x = 1 phase stabilizes into a brownmillerite structure, i.e., $SrCoO_{2.5}$ (SCO), because the Co^{4+} is a highly unstable valence state and the perovskite $SrCoO_3$ easily loses oxygen in ambient conditions [12,13]. Even with the same nominal Co valence state of 3+, brownmillerite SCO epitaxial thin films on STO substrates possess antiferromagnetic or nonmagnetic insulating ground states, possibly due to the drastic change in the crystal fields.

The heterointerface between transition metal oxides is an excellent platform for tailoring electromagnetic properties to obtain novel phenomena. While superlattices (SLs) composed of perovskite building blocks have been investigated the most, SLs composed of perovskite LCO and brownmillerite SCO can provide more insights into the magnetic properties of LSCO systems. The SLs are clearly distinguished from a solid solution where the chemical doping of Sr ions into LCO inevitably induce site disorder. A resulting inhomogeneity may

affect the magnetic exchange interactions by inducing broken paths of magnetic exchange interactions. In $(LaCoO_3)_n/(SrCoO_{2.5})_n$ SLs ($(LCO)_n/(SCO)_n$ SLs), because La and Sr ions are separated into layers by interfaces, the *A*-site disorder effect can be reduced significantly.

In this paper, we report the electrical, magnetic, and optical properties of $(LCO)_n/(SCO)_n$ SLs (n = 1, 2, 4, 10, and 20) grown on STO substrates. We find that variations in the periodicity n induce drastic changes in the electronic structure and, therefore, the magnetic properties. The n = 10 and 20 SLs are ferromagnetic with $T_C \sim 80$ K, similar to LCO thin films. This magnetization is largely suppressed in the n = 4 SL. For the n = 1 and 2 SLs, however, the system becomes ferromagnetic again, but with much higher T_C of 225 and 180 K, respectively. The comparison of the n = 1 SL and the $La_{1/3}Sr_{2/3}CoO_{3-\delta}$ thin film demonstrates that the former has superior magnetic properties, i.e., larger saturation magnetization, smaller coercive field, and higher T_C, although the nominal Sr concentration of the samples is the same. Optical conductivity $\sigma_1(\omega)$ data indicate that the evolution of the magnetic properties can be attributed to the spin-state transition with periodicity n. The $\sigma_1(\omega)$ data of the n = 10 and 20 SLs are very similar to those of LCO, which is dominated by an optical transition from O 2*p* to Co 3*d* e_g states at approximately 2.5 eV. With decreasing n, the spectral weight shifts to lower energies, forming intersite t_{2g} - t_{2g} excitations. The intersite excitations are strongly enhanced in the $\sigma_1(\omega)$ of the n = 1 and 2 SL samples, suggesting that the low-spin Co^{3+} ions in the large n SLs turn into high-spin ones. The periodicity dependence of the strength of the intersite excitations is found to correlate with those of the magnetic properties. We also note that the strength of the intersite transition of the n = 1 SL sample is larger than that of the corresponding $La_{1/3}Sr_{2/3}CoO_{3-\delta}$ thin film, which confirms the superiority of the ferromagnetic properties of the former. Our results suggest that $(LCO)_n/(SCO)_n$ SLs represent a novel platform to control the ferromagnetic properties of an insulator with suppressed *A*-site disorder.

II. EXPERIMENTS

We grew $(LCO)_n/(SCO)_n$ SLs (n = 1, 2, 4, 10, and 20) and $La_{1/3}Sr_{2/3}CoO_{3-\delta}$ thin films on STO (001) substrates using pulsed laser epitaxy (KrF, λ = 248 nm). A laser fluence of ~1

Jcm^{-2} and frequency of 10 Hz was used for ablating sintered LCO and SCO targets. The substrate temperature was 650 °C and the oxygen partial pressure was 100 mTorr. The growth condition was carefully selected to induce perovskite LCO and brownmillerite SCO phases [9,14,15].

To control the interface density, we fixed the total thicknesses of the $(LCO)_n/(SCO)_n$ SLs and $La_{1/3}Sr_{2/3}CoO_{3-\delta}$ thin films to ~72 nm, corresponding to 60 repetitions of each pseudocubic unit cell of LCO (~0.4 nm) and pseudotetragonal unit cell (one octahedral layer and one tetrahedral layer) of SCO (~0.8 nm along the growth direction, *c*-axis). The thickness is chosen to ensure enough repetition for the thick-layer superlattices, i.e., n = 10 and 20, which would lead to a systematic comparison among the superlattice samples. The symbol n represents the number of a unit cell of each layer in the SLs. Accordingly, the periodicity ratio of LCO and SCO is fixed to 1 : 1. Because the *c*-axis lattice constant of the pseudotetragonal unit cell of SCO is roughly twice that of the LCO, the thickness ratio of LCO to SCO is approximately 1 : 2 and the Sr concentration for the SLs is 2/3.

The sheet resistance as a function of temperature $R_s(T)$ was measured with a physical property measurement system using the Van der Pauw geometry with In electrodes. The magnetization as a function of temperature $M(T)$ and magnetic field $M(H)$ were measured using a superconducting quantum interference device. The magnetic field was applied to the in-plane direction of the SLs and thin films.

To study electronic responses, we measured the *ab*-plane reflectivity spectra $R(\omega)$ at energies between 10 meV and 1 eV, using a Fourier-transform infrared spectrometer (Bruker Vertex 70v). An *in-situ* gold overcoating technique was used to obtain accurate $R(\omega)$ data [16]. A liquid helium flow cryostat was used to measure $R(\omega)$ at 10 K. The optical conductivity $\sigma_1(\omega)$ spectra were obtained with a Drude-Lorentz oscillator fit of the reflectivity spectra. Because the penetration depth of the infrared light is much larger than the thickness of the samples, we approximated each SL as a single medium with effective dielectric constants [17]. In the energy region between 0.7 and 5.5 eV, we also employed a spectroscopic ellipsometer (VASE, J. A. Woollam Co.) to cross-check the optical spectra obtained by the $R(\omega)$ measurement.

III. RESULTS AND DISCUSSION

A. Atomic structure of $(LaCoO_3)_n/(SrCoO_{2.5})_n$ superlattices

Figures 1(a) and 1(b) show x-ray diffraction (XRD) θ-2θ scan patterns of the $(LCO)_n/(SCO)_n$ SLs and $La_{1/3}Sr_{2/3}CoO_{3-\delta}$ thin film and indicate that all the films are epitaxially grown with *c*-axis orientation. The narrow superlattice satellite peaks observed in the n = 4, 10, and 20 SL samples demonstrate the high quality of the SLs with atomically sharp interfaces. It should be pointed out that the half-order peaks corresponding to the brownmillerite SCO phase [12,14], labelled as BM-SCO in Fig. 1(a), appear in the n = 4 SL and become more evident with increasing n. It has been frequently discussed that the Co 4+ valence state in the perovskite $SrCoO_{3.0}$ phase is rather unstable, predominantly resulting in the brownmillerite phase of SCO without extra oxygen treatments using, e.g., ozone [14]. Indeed, it is clearly shown that, under the growth conditions of our experiment, the brownmillerite phase is preferred over the perovskite phase, especially for the SLs with large n. In those samples, we also observe the perovskite peaks, coming from the LCO layers, labelled as P-LCO. For the SLs with small n (1 and 2), the atomic ordering from the brownmillerite structure (alternating octahedral and tetrahedral layer) becomes less evident, leading to the disappearance of the half-order peaks. Figures 1(c) -1(e) display the representative x-ray reciprocal space maps (RSM) around the 103 Bragg reflection of the STO substrate. These data indicate that the SLs with n up to 20 are coherently grown as their in-plane lattice constants remain the same as that of the substrate. The coherent strain maintained up to a film thickness of ~70 nm is also a consequence of the alternating tensile strain (for LCO layers having a pseudo cubic lattice constant of 3.803 Å) and the absence of strain (for brownmillerite SCO layers having the same in-plane lattice constant as the STO substrate, i.e., 3.905 Å) within the SLs [12,17].

From the atomic structure of the $(LCO)_n/(SCO)_n$ SLs characterized by XRD, it can be inferred that the global valence state of the Co ions within and throughout the SLs is fixed to 3+. While the local structures and stacking sequences of the octahedral and tetrahedral layers in SCO are subjects of a future transmission electron microscopy experiments, the designed coherent valence state allows us to investigate the magnetic exchange interactions within the

same average spin structures. It should also be noted that the designed SLs have a systematically engineered interface density. Because the total thickness is fixed to be the same for all SLs, the interface density increases as the periodicity decreases.

B. Electrical and magnetic properties

Figure 2 shows the sheet resistance R_s of the $(LCO)_n/(SCO)_n$ SLs and the $La_{1/3}Sr_{2/3}CoO_{3-\delta}$ thin film as a function of temperature. All the samples show insulating behavior. While the nominal $La_{1/3}Sr_{2/3}CoO_3$ thin film with $\delta = 0$ should be metallic, the insulating temperature dependence is manifested as a large amount of oxygen vacancies, comparable to that of the SLs in the $La_{1/3}Sr_{2/3}CoO_{3-\delta}$ thin film. In the $(LCO)_n/(SCO)_n$ SLs, as the interface density decreases (or as n increases), the contribution from the interface will decrease and R_s should approach the parallel resistivities of LCO and SCO. Surprisingly, however, the electrical resistance does not follow a monotonic behavior with n. As n increases up to ~4, R_s decreases by more than 4 orders of magnitude at room temperature. As n increases further, R_s gradually increases again. A minimum in R_s is estimated around $n = 4$, implying a competition between the interface density and the dimensional effect in deciding the electronic ground state of the SLs.

The variation in the periodicity n induces an intriguing evolution of the magnetic state of the SLs, which follows the same trend as in the electrical resistivity. Figure 3 shows the temperature-dependent magnetization $M(T)$ at 1000 Oe and the magnetic-field-dependent magnetization $M(H)$ at 5 K of the SL samples. In the $n = 20$ SL, a ferromagnetic transition at $T_C \approx 80$ K is manifested in the $M(T)$ curve (see the inset in Fig. 3). Its $M(H)$ curve also shows a clear hysteresis loop below the T_C. This is consistent with the ferromagnetic transition in LCO thin films on STO substrates [7,18,19]. Because SCO is known to be antiferromagnetic or nonmagnetic, the magnetic properties of the LCO/SCO heterostructure with fairly thick constituent layers originate from the LCO layer alone. However, as n decreases, the interface density increases and the distinctive exchange across Sr and La becomes active. Resultantly, the $n = 4$ SL shows an almost nonmagnetic behavior with completely suppressed magnetic moment down to the lowest temperature (see the inset in Fig. 3). Only a weak paramagnetic

moment is observed in the $M(H)$ curve without hysteresis. Surprisingly, however, the ferromagnetic ground state is restored as n decreases further. For the n = 2 and 1 SLs, a clear ferromagnetic transition is observed in the $M(T)$ curves below T_C of ~180 and ~225 K, respectively. The magnetization of the small n SLs is much larger than that of the large n SLs. Notably, the n = 1 SL shows even larger magnetization and T_C (but smaller coercive field) compared to those of the $La_{1/3}Sr_{2/3}CoO_{3-\delta}$ thin film, although their nominal Sr concentrations are the same, indicating the importance of the layered structure design.

The magnetic state evolution of the SLs with n is reminiscent of that of $La_{1-x}Sr_xCoO_3$ thin films with hole doping due to the substitution of Sr^{2+} ions. The $La_{1-x}Sr_xCoO_3$ films grown on STO substrate with $x = 0$ and $x \geq 0.3$ display ferromagnetic order and their T_C are 80 and 250 K, respectively [19]. In the intermediate doping range of $0.05 < x < 0.2$, the ferromagnetic order almost disappears, leading to a nonmagnetic state ($x \sim 0.15$). However, in our SLs, because the nominal valence of Co ions is 3+ in both the LCO and SCO layers, charge doping should not be viable. The robust insulating behavior is also in stark contrast to that of $La_{1-x}Sr_xCoO_3$ films [20-24]. Instead, the dimensional and interface effects play more important roles in determining the magnetic properties of the SLs.

C. Optical response

To gain insight into the evolution of the magnetic ground state with n, we measured the optical responses of the SLs. Figure 4 displays the reflectivity $R(\omega)$ spectra of STO and $(LCO)_n/(SCO)_n$ SLs at 10 K. The spectral shape of the $R(\omega)$ of the n = 20 SL is nearly the same as that of the STO substrate at energies below 0.1 eV (Fig. 4(a)), indicating a negligible contribution from the SL, except for some phonon lines. At higher energies, $R(\omega)$ of the n = 20 SL shows a broad hump structure, in contrast to the flat spectral shape of the substrate. The shape of $R(\omega)$ of the SL progressively deviates from that of the substrate with decreasing n. Because the interface density increases with decreasing n, we conclude that the contribution from the interface of the SL screens the effect of the STO. We fit $R(\omega)$ using the Drude and Lorentz oscillator model to obtain optical conductivity data. The results of the fits are shown in red solid lines in Figs. 4(a)-4(f).

Figure 5 shows the real part of the optical conductivity $\sigma_1(\omega)$ of the $(LCO)_n/(SCO)_n$ SLs at 10 K. We observe that the $\sigma_1(\omega)$ spectra of the n = 10 and n = 20 SLs are very similar to those

of the LCO and SCO thin films but is in sharp contrast to that of the perovskite $SrCoO_3$ [25], revealing the brownmillerite $SrCoO_{2.5}$ phase within our SLs. The $\sigma_1(\omega)$ of the n = 10 and 20 SLs display three optical transitions at approximately 0.5 (α), 1.5 (β), and 3.0 (γ) eV. We note that the $\sigma_1(\omega)$ of the LCO thin film exhibits three absorption peaks at almost the same energies [26]. According to the dynamical mean field theory calculation on LCO films, the three peaks at ~0.5, ~1.5 and ~3.0 eV can be assigned to Co 3d t_{2g} – t_{2g}, Co 3d t_{2g} – e_g, and O 2p – Co 3d e_g transitions, respectively [26]. The higher energy absorption peaks can also be attributed to the Co d – d and O 2p – Co 3d transitions in the brownmillerite SCO at ~1.4 and ~2.8 eV, respectively [13,25]. Thus, the optical and magnetization data suggest that the effect of the interface is minimized by large periodicity n, and the optical responses of the n = 10 and 20 SLs are dominated by the inner layers of LCO and SCO.

As the periodicity n decreases from 10 to 4, the α and β peaks are enhanced and the γ peak is suppressed slightly, whereas overall spectral shape does not change significantly. However, further decrease in n down to 2 and 1 leads to a drastic variation in $\sigma_1(\omega)$. The α peak is strongly enhanced with the suppression of the γ peak and is shifted to a lower energy of approximately 0.3 eV, as shown in Fig. 5(b). We note that the $\sigma_1(\omega)$ of the n = 1 and 2 SLs cannot be reproduced by linear combinations of the $\sigma_1(\omega)$ of LCO and SCO. Thus, these changes should be attributed to the electronic reconstruction at the interface, as the relative ratio of the interface layer to the inner layer increases with decreasing n. Ideally, the n = 1 SL has only the interfacial layers and the Sr concentration should be 2/3. While the $\sigma_1(\omega)$ of the n = 1 SL is similar to that of the $La_{1/3}Sr_{2/3}CoO_{3-\delta}$ thin film in terms of optical transitions, one notable difference is that the α peak is even stronger in the n = 1 SL, which will be discussed later.

The $\sigma_1(\omega)$ of the n = 1 and 2 SLs are qualitatively different from those of hole-doped ferromagnetic $La_{1-x}Sr_xCoO_3$ crystals and thin films [22,24,27]. The latter compounds show metallic state and their ferromagnetic state is attributed to the double exchange interaction between the t_{2g} electrons of Co^{3+} and Co^{4+} ions [28-30]. In $\sigma_1(\omega)$ spectra, the metallicity is represented by a Drude-like peak centered at zero energy. However, a Drude-like peak is not observed in our SLs, which is consistent with their insulating behavior observed in the sheet resistance data. The sharp spikes near the zero energy are due to the infrared-active phonon mode. Instead, a strong peak at a finite energy (the α peak) is observed in the n = 1 and 2 SLs

and the $La_{1/3}Sr_{2/3}CoO_{3-\delta}$ thin film. Such a carrier localization can be attributed to the maintenance of the Co^{3+} valence state with the introduction of oxygen vacancies in our samples.

The changes in $\sigma_1(\omega)$ with n in conjunction with the magnetization data provide insights into the evolution of the spin configuration of the SLs with n. First, let us consider the n = 10 and 20 SLs. The resemblance of their $\sigma_1(\omega)$ and ferromagnetic properties with those of LCO epitaxial thin films suggests that the spin configuration of the n = 10 and 20 SLs may be composed of Co^{3+} high-spin (HS) and low-spin (LS) states and the superexchange interaction between the Co^{3+} HS and LS states within the LCO sublayer induces a ferromagnetic state, similar to that of epitaxial LCO thin films [28]. The band diagrams for Co^{3+} HS and LS states are drawn schematically in Fig. 5(c).

Despite the similarity of the spectral shapes of the $\sigma_1(\omega)$ of the n = 4 SL and the n = 10 and 20 SLs, the nonmagnetic property of the former suggests that the magnetic exchange in the LCO layer is strongly suppressed by the low dimensional effect and the presence of the interface. Dimensional instabilities with the absence of coherent out-of-plane exchange interactions suppress the spin ordering, despite the presence of the α peak in the $\sigma_1(\omega)$ of the n = 4 SL.

The variation in the $\sigma_1(\omega)$ with n decreasing from 4 to 2 and 1 suggests that a significant portion of the Co^{3+} LS states is converted into Co^{3+} HS states, as the interface density doubles and quadruples, respectively [31]. This spin-state transition involves the transfer of electrons from t_{2g} to e_g states, creating an unoccupied t_{2g} level, which in turn leads to the enhancement of the Co 3d t_{2g} (occupied e_g) – t_{2g} transition (α peak) as shown in Fig. 5(c). The LS-to-HS transition inferred from the optical data is also in line with the largely enhanced ferromagnetic behavior of the n = 2 and 1 SLs, of which T_C and the magnetizations are substantially higher than those of the n = 10 and 20 SLs.

The α peak in the $\sigma_1(\omega)$ spectra corresponds to the intersite Co t_{2g} – t_{2g} excitation and is associated with magnetic exchange interactions in our cobaltite SLs. We overlay the strength of the α peak obtained from the integration of $\sigma_1(\omega)$ in the energy region between 0.08 and 1 eV with R_s, T_C, remnant magnetization (M_r), and saturation magnetization (M_s) at 6 T in Fig. 6. We find that the evolution of the α peak with n follows the behavior of the magnetic characteristics. Such an interdependence supports the notion that the ferromagnetism in the

$(LCO)_n/(SCO)_n$ SLs is induced by the magnetic exchange interactions between the t_{2g} electrons of Co^{3+} ions. In Fig. 6, a stark distinction is manifested depending on the magnetic exchange mechanism with a reference point with n = 4 SL. For larger n, the exchange interactions between the HS and LS states of Co^{3+} ions in the LCO sublayer yields ferromagnetism [28]. On the other hand, for smaller n, the interlayer magnetic exchange interactions with mostly HS states of Co ions in the LCO and SCO sublayers may play an important role for their largely enhanced ferromagnetism.

Surprisingly, Figure 6 reveals a clear correlation between the electrical resistance and the magnetic properties. The enhancement of the ferromagnetism goes alongside the increase in the electrical resistance, which is most prominent in the n = 1 and 2 SLs. This is in stark contrast to the relationship between the magnetic and transport properties of hole-doped $La_{1-x}Sr_xCoO_3$ films, where itinerant carriers mediate ferromagnetic double exchange interactions [20-24]. The absence of anomalies at T_C in the temperature-dependent electrical resistance further indicates that the double exchange mechanism is not viable in our system. We speculate that the enhancement of the carrier scattering at the interfaces may be responsible for the increase in the resistance in the low-periodicity SLs, i.e., n = 1 and 2. The inference from our result that the properties of the superlattices are controlled by the interface density suggests that the trend revealed in Fig. 6 is likely to persist in thinner superlattice films with less repetition. In any case, such an unconventional trend in the coupling between ferromagnetism and insulating properties is highly beneficial in actual realization of robust ferromagnetic insulators.

We finally discuss the quantitative difference between the strength of the α peak of the n = 1 SL and the $La_{1/3}Sr_{2/3}CoO_{3-\delta}$ thin films. As shown in Fig. 5(b), although the nominal Sr concentration is the same in both samples, the α peak in the $\sigma_1(\omega)$ of the n = 1 SL is much stronger than that of the $La_{1/3}Sr_{2/3}CoO_{3-\delta}$ thin film, which is consistent with the higher T_c and magnetization value of the former. The A-site disorder in the SL is lower than that in the $La_{1/3}Sr_{2/3}CoO_{3-\delta}$ thin film because the LCO and SCO layers are stacked alternately. We suggest that the weaker A-site disorder may contribute to the increase in the number of channels of the Co $t_{2g} - t_{2g}$ excitations in the n = 1 SL, thus leading to the enhancement of the α peak, T_c, and magnetization value.

IV. SUMMARY

In summary, we have shown that the ferromagnetic properties of the insulating $(LaCoO_3)_n/(SrCoO_{2.5})_n$ SLs (n = 1, 2, 4, 10, and 20) can be controlled by changing their periodicity n. We find that the n = 10 and 20 SLs are ferromagnetic with $T_C \sim 80$ K, similar to the $LaCoO_3$ thin films. The n = 4 SL is almost nonmagnetic. The n = 1 and 2 SLs are found to be ferromagnetic with T_C of approximately 225 and 180 K, respectively. The value of the magnetization of the n = 1 and 2 SLs are larger than those of the n = 10 and 20 SLs by more than a factor of 10, suggesting a stark distinction between the magnetic exchange mechanisms of the small and large n SLs. The comparison of the n = 1 SL, with a nominal Sr concentration of 2/3, and the $La_{1/3}Sr_{2/3}CoO_{3-\delta}$ film reveals that the former has superior magnetic properties, i.e., larger saturation magnetization, smaller coercive field, and higher T_C. The optical conductivity of the n = 10 and 20 SLs are similar to those of the $LaCoO_3$ and brownmillerite $SrCoO_{2.5}$, which are dominated by an optical transition from the O 2p to the Co e_g state at approximately 2.5 eV. With n decreasing to 1, the spectral weight shifts to lower energies and the $t_{2g} - t_{2g}$ intersite optical transition at approximately 0.5 eV is enhanced. We find a close interdependence between the periodicity dependences of the magnetic properties, electrical resistance, and strength of the $t_{2g} - t_{2g}$ intersite excitation. Our results suggest that the $(LaCoO_3)_n/(SrCoO_{2.5})_n$ SLs represent a novel system to manipulate the magnetism of the cobaltite compounds.

ACKNOWLEDGMENTS

This research was supported by the Basic Science Research Program through the National Research Foundation of Korea (NRF) funded by the Ministry of Science, ICT and Future Planning (Grant No. 2017R1A2B4009413 and 2019R1A2B5B02004546). The work was also supported by the U.S. Department of Energy, Office of Science, Basic Energy Sciences, Materials Sciences and Engineering Division. The magnetic measurements were conducted at the Center for Nanophase Materials Sciences, which is a DOE Office of Science User Facility. This work was supported by LG Yonam Foundation.

[1] K. Uchida, J. Xiao, H. Adachi, J. Ohe, S. Takahashi, J. Ieda, T. Ota, Y. Kajiwara, H. Umezawa, H. Kawai, G. E. Bauer, S. Maekawa, and E. Saitoh, Spin Seebeck insulator, Nat. Mater. **9**, 894 (2010).

[2] Z. Wang, Y. Sun, M. Wu, V. Tiberkevich, and A. Slavin, Control of spin waves in a thin film ferromagnetic insulator through interfacial spin scattering, Phys. Rev. Lett. **107**, 146602 (2011).

[3] J. A. C. Bland, T. Taniyama, W. S. Cho, and S. J. Steinmueller, Spin selective transport at the ferromagnet/semiconductor interface, Curr. Appl. Phys. **3**, 429 (2003).

[4] Z. Wang, C. Tang, R. Sachs, Y. Barlas, and J. Shi, Proximity-induced ferromagnetism in graphene revealed by the anomalous Hall effect, Phys. Rev. Lett. **114**, 016603 (2015).

[5] B. F. Miao, S. Y. Huang, D. Qu, and C. L. Chien, Physical origins of the new magnetoresistance in Pt/YIG, Phys. Rev. Lett. **112**, 236601 (2014).

[6] D. Fuchs, E. Arac, C. Pinta, S. Schuppler, R. Schneider, and H. v. Löhneysen, Tuning the magnetic properties of $LaCoO_3$ thin films by epitaxial strain, Phys. Rev. B **77**, 014434 (2008).

[7] D. Fuchs, C. Pinta, T. Schwarz, P. Schweiss, P. Nagel, S. Schuppler, R. Schneider, M. Merz, G. Roth, and H. v. Löhneysen, Ferromagnetic order in epitaxially strained $LaCoO_3$ thin films, Phys. Rev. B **75**, 144402 (2007).

[8] Y. Li, S. J. Peng, D. J. Wang, K. M. Wu, and S. H. Wang, Strain effect on the magnetic and transport properties of $LaCoO_3$ thin films, AIP Advances **8** (2018).

[9] W. S. Choi, J. H. Kwon, H. Jeen, J. E. Hamann-Borrero, A. Radi, S. Macke, R. Sutarto, F. He, G. A. Sawatzky, V. Hinkov, M. Kim, and H. N. Lee, Strain-induced spin states in atomically ordered cobaltites, Nano Lett. **12**, 4966 (2012).

[10] J. M. Rondinelli and N. A. Spaldin, Structural effects on the spin-state transition in epitaxially strained $LaCoO_3$ films, Phys. Rev. B **79**, 054409 (2009).

[11] D. Meng, H. Guo, Z. Cui, C. Ma, J. Zhao, J. Lu, H. Xu, Z. Wang, X. Hu, Z. Fu, R. Peng, J. Guo, X. Zhai, G. J. Brown, R. Knize, and Y. Lu, Strain-induced high-temperature perovskite ferromagetic insulator, Proc. Natl. Acad. Sci. U. S. A. **115**, 2873 (2018).

[12] H. Jeen, W. S. Choi, J. W. Freeland, H. Ohta, C. U. Jung, and H. N. Lee, Topotactic phase transformation of the brownmillerite $SrCoO_{2.5}$ to the perovskite $SrCoO_{3-\delta}$, Adv. Mat. **25**, 3651 (2013).

[13] J. H. Lee, W. S. Choi, H. Jeen, H. J. Lee, J. H. Seo, J. Nam, M. S. Yeom, and H. N. Lee, Strongly coupled magnetic and electronic transitions in multivalent strontium cobaltites, Sci. Rep. **7**, 16066 (2017).

[14] H. Jeen, W. S. Choi, M. D. Biegalski, C. M. Folkman, I. C. Tung, D. D. Fong, J. W. Freeland, D. Shin, H. Ohta, M. F. Chisholm, and H. N. Lee, Reversible redox reactions in an epitaxially stabilized $SrCoO_x$ oxygen sponge, Nat. Mater. **12**, 1057 (2013).

[15] W. S. Choi, K. T. Kang, H. Jeen, Z. Gai, and H. N. Lee, Highly insulating ferromagnetic cobaltite heterostructures, Curr. Appl. Phys. **17**, 722 (2017).

[16] C. C. Homes, M. Reedyk, D. A. Cradles, and T. Timusk, Technique for measuring the reflectance of irregular, submillimeter-sized samples, Appl. Opt. **32**, 2976 (1993).

[17] D. W. Jeong, W. S. Choi, T. D. Kang, C. H. Sohn, A. David, H. Rotella, A. A. Sirenko, C. H. Lee, J. H. Kim, U. Lüders, W. Prellier, Y. J. Kim, Y. S. Lee, and T. W. Noh, Optical spectroscopy of the carrier dynamics in $LaVO_3/SrVO_3$ superlattices, Phys. Rev. B **84**, 115132 (2011).

[18] C. Pinta, D. Fuchs, M. Merz, M. Wissinger, E. Arac, H. v. Löhneysen, A. Samartsev, P. Nagel, and S. Schuppler, Suppression of spin-state transition in epitaxially strained $LaCoO_3$, Phys. Rev. B **78**, 174402 (2008).

[19] H. W. Yang, H. R. Zhang, Y. Li, S. F. Wang, X. Shen, Q. Q. Lan, S. Meng, R. C. Yu, B. G. Shen, and J. R. Sun, Anomalous magnetism in strained $La_{1-x}Sr_xCoO_3$ epitaxial films ($0 \leq x \leq 0.5$), Sci. Rep. **4**, 6206 (2014).

[20] Y. Tokura, Y. Okimoto, S. Yamaguchi, and H. Taniguchi, Thermally induced insulator-metal transition in $LaCoO_3$: A view based on the Mott transition, Phy. Rev. B (R) **58**, 1699 (1998).

[21] M. Itoh, I. Natori, S. Kubota, and K. Motoya, Spin-glass behavior and magnetic phase diagram of $La_{1-x}Sr_xCoO_3$ ($0 \leq x \leq 0.5$) studied by magnetization measurement, J. Phys. Soc. Jpn. **63**, 1468 (1994).

[22] M. A. Señarís-Rodríguez and J. B. Goodenough, Magnetic and transport properties of the system $La_{1-x}Sr_xCoO_{3-\delta}$ ($0 < x \leq 0.5$), J. Solid State. Chem. **118**, 323 (1995).

[23] W. Y. Cui, P. Li, and H. L. Bai, Spin-state configuration induced faster spin dynamics in epitaxial $La_{1-x}Sr_xCoO_3$ thin films, Solid State Commun. **209**, 49 (2015).

[24] B. Liu, Y. Wang, G. Liu, H. Feng, H. Yang, and J. Sun, Electrical transport properties of $La_{1-x}Sr_xCoO_3$ thin films, J. Appl. Phys. **120** (2016).

[25] W. S. Choi, H. Jeen, J. H. Lee, S. S. Seo, V. R. Cooper, K. M. Rabe, and H. N. Lee, Reversal of the lattice structure in $SrCoO_x$ epitaxial thin films studied by real-time optical spectroscopy and first-principles calculations, Phys. Rev. Lett. **111**, 097401 (2013).

[26] D. W. Jeong, W. S. Choi, S. Okamoto, J. Y. Kim, K. W. Kim, S. J. Moon, D. Y. Cho, H. N. Lee, and T. W. Noh, Dimensionality control of *d*-orbital occupation in oxide superlattices, Sci. Rep. **4**, 6124 (2014).

[27] H. M. Aarbogh, J. Wu, L. Wang, H. Zheng, J. F. Mitchell, and C. Leighton, Magnetic and electronic properties of $La_{1-x}Sr_xCoO_3$ single crystals across the percolation metal-insulator transition, Phys. Rev. B **74** (2006).

[28] M. Merz, P. Nagel, C. Pinta, A. Samartsev, H. v. Löhneysen, M. Wissinger, S. Uebe, A. Assmann, D. Fuchs, and S. Schuppler, X-ray absorption and magnetic circular dichroism of $LaCoO_3$, $La_{0.7}Ce_{0.3}CoO_3$, and $La_{0.7}Sr_{0.3}CoO_3$ films: Evidence for cobalt-valence-dependent

magnetism, Phys. Rev. B **82**, 174416 (2010).

[29] D. Fuchs, M. Merz, P. Nagel, R. Schneider, S. Schuppler, and H. von Lohneysen, Double exchange via t_{2g} orbitals and the Jahn-Teller effect in ferromagnetic $La_{0.7}Sr_{0.3}CoO_3$ probed by epitaxial strain, Phys. Rev. Lett. **111**, 257203 (2013).

[30] P. Friš, D. Munzar, O. Caha, and A. Dubroka, Direct observation of double exchange in ferromagnetic $La_{0.7}Sr_{0.3}CoO_3$ by broadband ellipsometry, Phys. Rev. B **97**, 045137 (2018).

[31] In the n = 1 and 2 SLs, quantum size effects might give rise to exotic effects in the elctronic structure. However, the qualitative similarity between $\sigma_1(\omega)$ of the n = 1, 2 SLs and the $La_{1/3}Sr_{2/3}CoO_{3-\delta}$ films suggests that the quantum confinement effects might not be strong enough to alter the electronic structure drastically.

Figure captions

FIG. 1. (a)-(b) X-ray diffraction (XRD) θ-2θ scan data of $(LaCoO_3)_n/(SrCoO_{2.5})_n$ SLs and $La_{1/3}Sr_{2/3}CoO_{3-\delta}$ thin film. BM and P indicate brownmillerite and perovskite structures, respectively. (c)-(e) X-ray reciprocal space maps of the n = 4, 10, and 20 SLs around the 103 Bragg reflection of the STO substrate, respectively.

FIG. 2. Sheet resistance of $(LCO)_n/(SCO)_n$ SLs and $La_{1/3}Sr_{2/3}CO_{3-\delta}$ thin film.

FIG. 3. (a) Temperature-dependent magnetization $M(T)$ and (b) isothermal magnetization $M(H)$ curves of $(LCO)_n/(SCO)_n$ SLs and $La_{1/3}Sr_{2/3}CO_{3-\delta}$ thin film at 5 K. The inset in (a) shows the magnified view of the $M(T)$ of the n = 4, 10, and 20 SLs.

FIG. 4. Reflectivity $R(\omega)$ spectra of (a) STO substrate, (b) n = 20, (c) n = 10, (d) n = 4, (e) n = 2, and (f) n = 1 SLs at 10 K. Open circle and red line represent experimental and fitted $R(\omega)$, respectively.

FIG. 5. (a)-(b) Real part of the optical conductivity spectra $\sigma_1(\omega)$ of the $(LCO)_n/(SCO)_n$ SLs and $La_{1/3}Sr_{2/3}CO_{3-\delta}$ thin film. For comparison, we display $\sigma_1(\omega)$ of LCO (Ref. [26]) and brownmillerite $SrCoO_{2.5}$ (Ref. [13]) in (a). The sharp spikes near the zero energy are due to the infrared-active phonon mode. Inset of (a) show Lorentz oscillators corresponding to the α, β, and γ peaks for the n = 4 SL. (c) Schematic band diagrams of high-spin (HS) and low-spin (LS) Co^{3+} ion in the $(LCO)_n/(SCO)_n$ SLs.

FIG. 6. Sheet resistance (R_s) at 300 K, remnant magnetization (M_r), saturation magnetization at 6 T (M_s) at 5 K, Curie temperature (T_C) and spectral weight (SW) of the α peak in $\sigma_1(\omega)$ at 10 K of the $(LCO)_n/(SCO)_n$ SLs. The spectral weight of the α peak is obtained by integrating $\sigma_1(\omega)$ between 0.08 and 1 eV. The dashed vertical line at n = 4 represents the boundary between two distinct ferromagnetic regimes. The exchange interactions between Co^{3+} high-spin (HS) states are dominant at n < 4, whereas the exchange interactions between Co^{3+} high-spin and low-spin (HS+LS) states are dominant at n > 4. Blue and red dotted lines are guide to the eyes.

FIG. 1.

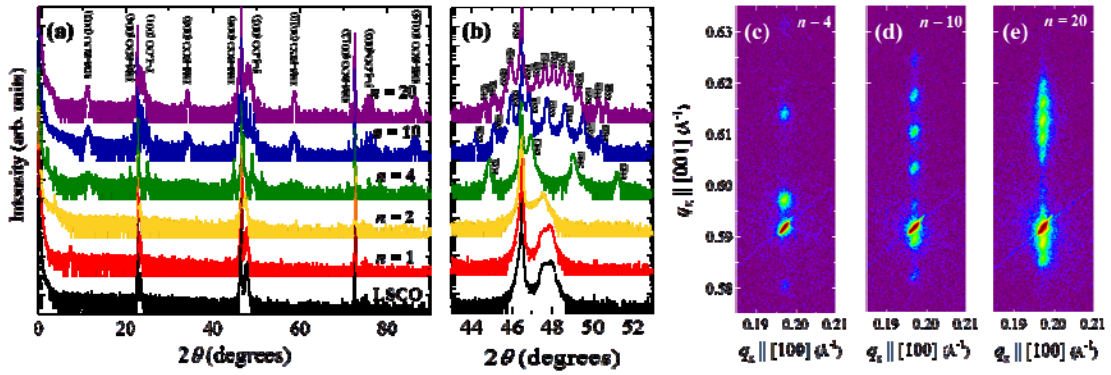
(a)
(b)
(c)
(d)
(e)
Intensity (arb. units)
2θ (degrees)
2θ (degrees)
n = 20
n = 10
n = 4
n = 2
n = 1
LSCO
n = 4
n = 10
n = 20
q_z ∥ [001] (Å^-1)
q_x ∥ [100] (Å^-1)
q_x ∥ [100] (Å^-1)
q_x ∥ [100] (Å^-1)

FIG. 2

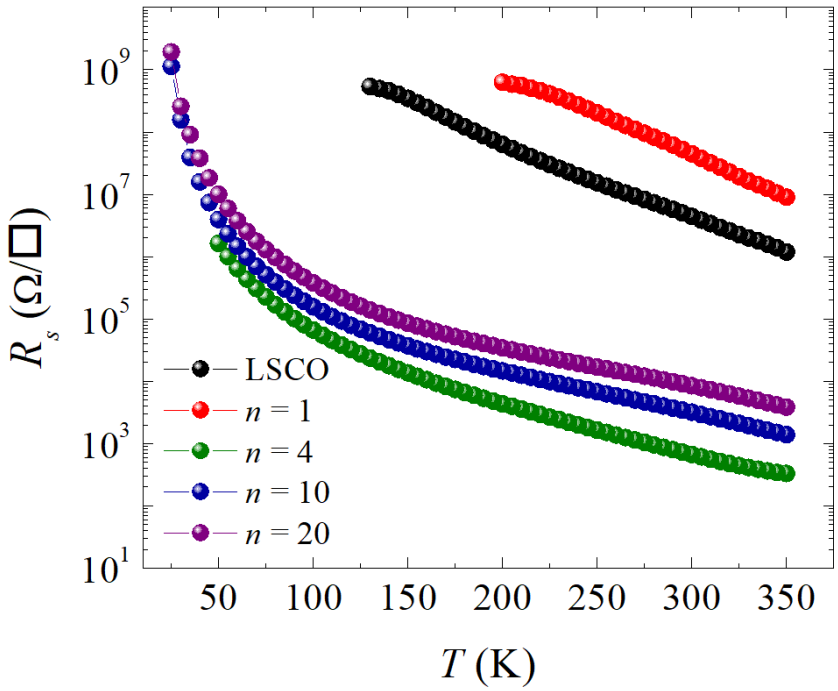
R_s (Ω/□)
T (K)
LSCO
n = 1
n = 4
n = 10
n = 20

FIG. 3

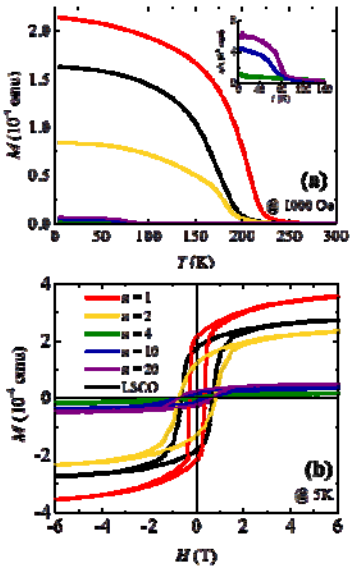
M (10⁻³ emu)
T (K)
(a)
@ 1000 Oe
n = 1
n = 2
n = 4
n = 10
n = 20
LSCO
M (10⁻⁴ emu)
H (T)
(b)
@ 5K

FIG. 4

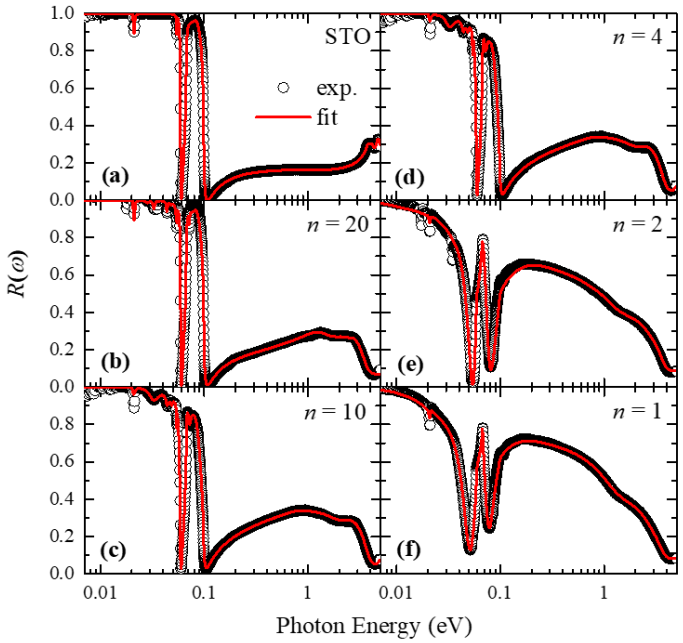
STO
exp.
fit
n = 4
n = 20
n = 2
n = 10
n = 1
(a)
(b)
(c)
(d)
(e)
(f)
R(ω)
Photon Energy (eV)

FIG. 5

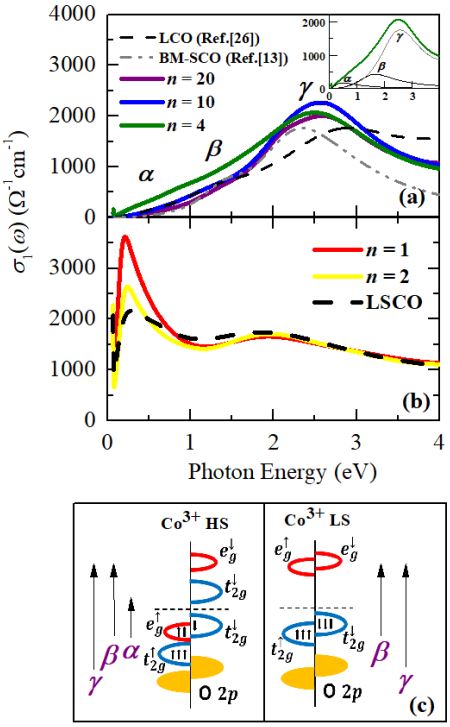
LCO (Ref.[26])
BM-SCO (Ref.[13])
n = 20
n = 10
n = 4
α
β
γ
(a)
n = 1
n = 2
LSCO
(b)
Photon Energy (eV)
σ1(ω) (Ω-1cm-1)
Co3+ HS
Co3+ LS
O 2p
(c)

FIG. 6

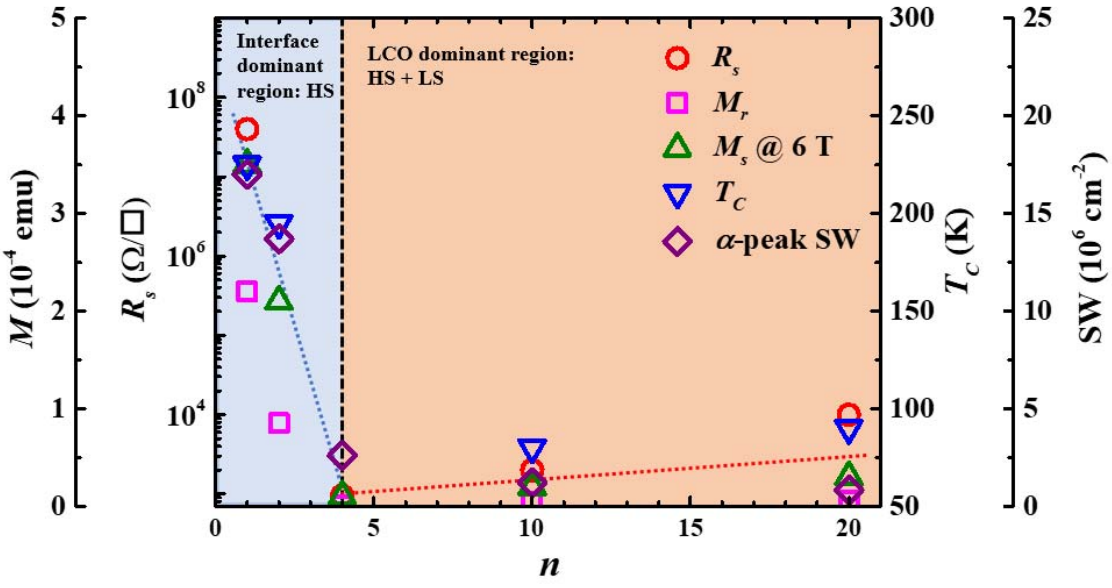
Interface dominant region: HS
LCO dominant region: HS + LS
Rs
Mr
Ms @ 6 T
TC
α-peak SW
M (10-4 emu)
Rs (Ω/□)
TC (K)
SW (10^6 cm-2)
n